Single-electron capture by Ar^{2+} from atomic and molecular targets

J. Phys. B: At. Mol. Phys. **20** (1987) 4129-4142. Printed in the UK

Single-electron capture by Ar^{2+} from atomic and molecular targets

E Y Kamber†, P Jonathan‡, A G Brenton‡ and J H Beynon‡

† Department of Physics, Kansas State University, Cardwell Hall, Manhattan, Kansas 66506, USA

‡ Mass Spectrometry Research Unit, University College Swansea, Singleton Park, Swansea SA2 8PP, UK

Received 5 September 1986, in final form 30 March 1987

Abstract. Translational-energy spectra for state-selective single-electron capture by Ar^{2+} from atomic (He, Ne, Ar, Kr, Xe) and molecular (N_2, O_2, NO, N_2O, NH_3, CO_2, CH_4, C_2H_6, 1-C_4H_8, C_6H_6) target gases are recorded at 6 keV impact energy using a reversed-geometry double-focusing mass spectrometer. Spectra indicate the presence of the ^3P, ^1D and higher excited states of Ar^{2+}, the populations of which are controlled by varying the ionising electron energy E_e. For Ar^{2+}-He at $E_e = 70$ eV, capture from the first excited ^1D state of Ar^{2+} into the ground state Ar^+ is most intense, whereas at $E_e = 43$ eV, ground state to ground state capture dominates. For Ar^{2+}-rare-gas systems, relative cross sections are discussed in terms of calculated reaction windows. For molecular targets, dissociation is evident in many cases. Broad peaks and long tails in the translational energy spectra indicate reaction channels involving closely spaced energy levels. An additional peak due to the capture of delocalised electrons is observed for unsaturated hydrocarbons which has not been previously reported.

1. Introduction and experimental technique

State-selective electron capture processes are of importance in applications to the production and diagnosis of state-selected ion beams, high-temperature plasmas and the determination of the emissivity and ionised structure of a wide variety of astrophysical species (Butler *et al* 1980).

Translational-energy spectroscopy has been extensively used to study state-selective electron capture by doubly charged argon ions in collision with rare-gas atoms in the collision-energy range from 140 eV to 6 keV (Ast *et al* 1975, Huber 1980, Kamber *et al* 1982a, b, Lennon *et al* 1983, Stevens *et al* 1983, Huber and Kahlert 1983, Jellen-Wutte *et al* 1985). The only detailed study of electron capture by Ar^{2+} ions from molecular targets that has been made is that of Neuschäfer *et al* (1979) for collisions of Ar^{2+} ions with N_2 at impact energies of 2, 15 and 25 eV in the centre of mass frame.

In the present work, we have studied the state-selective single-electron capture by 6 keV Ar^{2+} from rare-gas atoms (He, Ne, Ar, Kr, Xe) and molecular targets (N_2, O_2, NO, CO_2, N_2O, CH_4, C_6H_6, NH_3, C_2H_6, 1-C_4H_8). The data were obtained on a reversed-geometry double-focusing mass spectrometer (Morgan *et al* 1978). The doubly charged argon ions formed in an electron impact source, with an electron energy of 100(±2.5) eV, are extracted and accelerated through a potential of 3 kV. Ions are mass selected by the magnetic sector and introduced into a collision cell located at the

0022-3700/87/164129+14$02.50

intermediate focal point of the mass spectrometer. The translational-energy spectra were obtained under high energy resolution by scanning the voltage applied to the plates of the electrostatic analyser, situated after the collision cell. The energy resolution of the primary Ar^{2+} beam was 0.3 eV (FWHM).

Following the nomenclature described by Kamber *et al* 1982a, the observed reaction channels are given the folowing designations: I, II and III indicate the ground ($3p^4\ ^3P$) and metastable ($3p^4\ ^1D$, $3p^4\ ^1S$) states of the incident Ar^{2+} ions respectively; $\alpha, \beta, \gamma, \ldots$ represent the ground and successive excited states of the product Ar^+, respectively. X, A, B, ... represent the ground and successive excited states of the target product as indicated in tables 1 and 3, whereas Y represents target double ionisation. Dissociation of the molecular target ion may also be involved and we have used the symbols

Table 1. (a) Description and nomenclature of Ar ionic states. (*b*) Description and nomenclature of ionised rare-gas-target states.

(*a*)

Projectile Ar^{2+}		Ar^+ after capture	
State	Symbol	State	Symbol
$3p^4\ ^3P_2$	I	$3p^5\ ^2P^o_{3/2}$	α
$3p^4\ ^1D_2$	II	$3p^6\ ^2S_{1/2}$	β
$3p^4\ ^1S_0$	III	$3d\ ^4D_{7/2}$	γ
		$4s\ ^4P_{5/2}$	δ
		$4s\ ^2P_{3/2}$	ε

(*b*)

	Target T					
State	He	Ne	Ar	Kr	Xe	Symbol
Ground T^+	1s	$2p^5\ ^2P^o_{3/2}$	$3p^5\ ^2P^o_{3/2}$	$4p^5\ ^2P^o_{3/2}$	$5p^5\ ^2P^o_{3/2}$	X
1st exc. T^+	2p	$2p^6\ ^2S_{1/2}$	$3p^6\ ^2S_{1/2}$	$4p^6\ ^2S_{1/2}$	$5p^6\ ^2S_{1/2}$	A
2nd exc. T^+	3p	$3s\ ^4P^o_{5/2}$	$3d\ ^4D_{7/2}$	$5s\ ^4P_{5/2}$	$6s\ ^4P_{5/2}$	B
Ground T^{2+}		$2p^4\ ^3P_2$	$3p^4\ ^3P_2$	$4p^4\ ^3P_2$	$5p^4\ ^3P_2$	Y

Table 2. Threshold dissociation energies of target species for the formation of ionic products (relative to the neutral ground state).

Target	D_1	Energy (eV)	D_2	Energy (eV)	D_3	Energy (eV)
N_2	$N^+(^3P)+N(^4S^o)$	24.3	$N^+(^1D)+N(^4S^o)$	26.2	$N^+(^3P)+N(^2D^o)$	26.7
O_2	$O^+(^4S^o)+O(^3P)$	18.7	$O^+(^4S^o)+O(^1D)$	20.7	$O^+(^2D^o)+O(^3P)$	22
NO	$O^+(^4S^o)+N^+(^4S^o)$	20.1	$N^+(^3P)+O(^3P)$	21		
N_2O	$NO^+ + N$	15-16	$O^+ + N_2$	15-16	$N_2^+ + O$	>18
NH_3	$NH_2^+ + H$	15	$NH^+ + H_2$	17.2	$N^+ + H + H_2$	~22
CO_2	$O^+ + CO$	19.1	$CO^+ + O$	19.4	$C^+ + O_2$	~23
CH_4	$CH_3^+ + H$	14.4	$CH_2^+ + H_2$	15.3	$H^+ + CH_3$	21.3
C_2H_6	$C_2H_5^+ + H$	12	$C_2H_4^+ + H_2$	12.1	$CH_3^+ + CH_3$	14.1
1-C_4H_8	$C_3H_5^+ + CH_3$	11.8	$CH_3^+ + C_3H_5$	14.1		
C_6H_6	$C_6H_5^+ + H$	13.7	$C_4H_4^+ + C_2H_2$	13.9	$C_6H_4^+ + H_2$	14.1

Table 3. Description and nomenclature of ionised molecular-target states (first row for each target; ordering assumes Franck–Condon transitions) and excitation energies (in eV) relative to the neutral ground state for the ionised target species (second row for each target).

	State T^+			
Target T	Ground (X)	1st exc. (A)	2nd exc. (B)	3rd exc. (C)
N_2	$^2\Sigma_g^+$	$^2\Pi_u$	$^2\Sigma_u^+$	$^4\Sigma_u^+$
	15.6	17.0	18.8	21
O_2	$^2\Pi_g$	$^4\Pi_u$	$^2\Pi_u$	$^4\Sigma_g^-$
	12.3	16.6	17.5	18.2
NO	$^1\Sigma^+$	$^3\Sigma^+$	$^3\Pi$	$^3\Delta$
	9.3	16.1	16.6	17.3
N_2O	$^2\Pi$	$^2\Sigma^+$	$^2\Pi$	$^2\Sigma^+$
	12.9	16.4	18.2	20.1
NH_3	A′	^{2}E′†	—	—
	10.9	15.8	16.5	—
CO_2	$^2\Pi_g$	$^2\Pi_u$	$^2\Sigma_u^+$	$^2\Sigma_g^+$
	13.8	17.6	18.1	19.4
CH_4		^2T_g‡		$^2A_1$
	13.6	14.4	15	22.9
C_2H_6	^2E_g	^2A_g	^2E_u	^2A_u
	12.0	13.5	15.2	20.1
1-C_4H_8§	—	—	—	—
	9.4	11.8	12.8	13.2
C_6H_6	$1e_{1g}$	$3e_{2g}$	$1a_{2u}$	$3e_{1u}$
	9.3	11.5	12.4	14.0

† The general assignment of ^{2}E′ has been made since two vertical energies have been cited by Kimura *et al* (1981).

‡ The general assignment of ^2T_g has been made since two vertical energies have been cited by Kimura *et al* (1981).

§ Excited electronic states of this target are estimated from photoelectron spectra for its C_4H_8 isomers (see Kimura *et al* 1981).

$D_1, D_2, D_3, \ldots$ (refer to table 3) to denote successive dissociation levels. A single dissociation limit may be correlated to more than one molecular ion state, but the present experiment cannot distinguish these. The energy defect tables for the dissociative channels have been compiled using the asymptotic values of the first three lowest dissociation levels, which reflects the uncertainty in precisely defining this mechanism. Dissociation from an ion may occur directly from an excited state, either along one of the symmetry coordinates, or by coupling with a directly dissociative state of different multiplicity by spin–orbit interaction, or by more complicated trajectories involving conical intersections, or by vibrational/rotational coupling of the excited state with, for example, the ground-state vibrational manifold. In general, the dissociation energies, listed in table 2, have been obtained from appearance energy measurements (for example, from the compilation of Levin and Lias (1982)).

The possible outgoing channels following single-electron capture are listed in tables 4 and 5. The ionic energy levels used in preparing the tables are taken from Moore

Table 4. Energy defects for Ar^{2+}-rare-gas collision systems.

	Target				
Channel	He	Ne	Ar	Kr	Xe
$I\alpha X$	3.04	6.06	11.86	13.63	15.49
$I\beta X$	−10.43	−7.41	−1.61	0.16	2.02
$I\gamma X$	−13.36	−10.34	−4.54	−2.77	−0.91
$I\delta X$	−13.60	−10.58	−4.78	−3.01	−1.15
$I\varepsilon X$	−14.10	−11.08	−5.28	−3.51	−1.61
$I\zeta X$	−14.59	−11.57	−5.77	−4.00	−2.10
$I\eta X$			−6.56		
$I\alpha A$		−20.85	−1.62	0.12	4.23
$I\alpha B$			−4.55	−0.36	3.96
$I\alpha Y$			−15.76	−10.93	−5.71
$II\alpha X$	4.78	7.8	13.6	15.37	17.23
$II\beta X$	−8.69	−5.67	0.13	1.9	3.76
$II\gamma X$	−11.62	−8.60	−2.8	−1.03	0.83
$II\delta X$	−11.86	−8.84	−3.04	−1.27	0.59
$II\varepsilon X$	−12.36	−9.34	−3.54	−1.77	0.09
$II\alpha A$		−19.11	0.13	1.86	5.97
$II\alpha B$			−2.80	1.38	5.70
$II\alpha Y$			−14.02	−9.19	−3.97
$III\alpha X$	+7.16	10.18	15.98	17.75	19.61
$III\beta X$	−6.31	−3.8	2.51	4.28	6.14
$III\gamma X$	−9.24	−6.22	−0.42	1.35	3.21
$III\delta X$	−9.48	−6.45	−0.66	1.11	2.97
$III\varepsilon X$	−9.98	−6.96	−1.65	0.61	2.47
$III\alpha A$		−16.73	2.51	4.24	8.34
$III\alpha B$			−0.42	3.76	8.07
$III\alpha Y$			−11.64	−6.81	−1.59

(1971) for the rare gases, and for molecular targets from photoelectron spectra (Kimura *et al* 1981, Turner *et al* 1970, Robinson 1974, Eland 1984, Rabalais 1977) and ionisation and appearance energy measurements (Levin and Lias 1982). For molecular targets, formation of the ground state and the first three excited states has only been considered. Excitation has been assumed to be vertical and the molecular states used are listed in table 3. Interpretation of the excited states can be further complicated by the Jahn-Teller effect; methane, ammonia and ethane are three classic examples (Rabalais 1977). In these cases, the assignments and vertical energies quoted by Kimura *et al* (1981) have been used. Energy defects from double ionisation of molecular targets are not tabulated as these processes may only make minor contributions to the long, low intensity tail on the low-energy side of the spectra.

2. Results and discussion

2.1. Ar^{2+}-rare-gas collision systems

Single-electron capture by Ar^{2+} from He, Ne, Ar, Kr and Xe is possible via a number of competing reaction channels, the energy defects (ΔE) for which are given in table 4.

Table 5. Energy defects for Ar^{2+}-molecular-target collision systems.

	Target									
Channel	N_2	O_2	NO	N_2O	NH_3	CO_2	CH_4	C_2H_6	1-C_4H_8	C_6H_6
IαX	12.0	15.3	18.3	14.7	16.7	13.8	14.0	15.6	17.8	18.3
IβX	−1.5	1.8	4.8	1.2	3.2	0.3	0.5	2.1	4.3	4.8
IγX	−4.4	−1.1	1.9	−1.7	0.3	−2.6	−2.4	−0.8	1.4	1.9
IδX	−4.6	−1.3	1.7	−1.9	0.1	−2.8	−2.6	−1.0	1.2	1.7
IεX	−5.1	−1.8	1.2	−2.4	−0.4	−3.3	−3.1	−1.5	0.7	1.2
IζX	−5.6	−2.3	0.7	−2.9	−0.9	−3.8	−3.6	−2.0	0.2	0.7
IαA	10.6	11.0	11.5	11.2	11.8	10.0	13.2	14.1	15.8	16.1
IβA	−2.9	−2.5	−2.0	−2.3	−1.7	−3.5	−0.3	0.6	2.3	2.6
IαB	8.8	10.1	11.0	9.4	11.1	9.5	12.6	12.4	14.8	15.2
IαC	6.6	9.4	10.3	7.5	—	8.2	4.7	7.5	14.4	13.6
I$\alpha$$D_1$	3.3	8.9	7.5	12.1	12.6	8.5	13.2	15.6	15.8	13.9
I$\beta$$D_1$			−6.0							
I$\alpha$$D_2$	1.4	6.9	6.6	12.1	10.4	8.2	12.3	15.5	13.5	13.7
I$\alpha$$D_3$	0.9	5.6	—	9.6	5.6	4.6	6.3	13.5	—	13.5
IIαX	13.7	17.0	20.0	16.4	18.4	15.5	15.7	17.3	19.5	20.0
IIβX	0.2	3.5	6.5	2.9	4.9	2.0	2.2	3.8	6.0	6.5
IIγX	−2.7	0.6	3.6	0.0	2.0	−0.9	−0.7	0.9	3.1	3.6
IIδX	−2.9	0.4	3.4	−0.2	1.8	−1.1	−0.9	0.7	2.9	3.4
IIαA	12.3	12.7	13.2	12.9	13.5	11.7	14.9	15.8	17.5	17.8
IIβA	−1.2	−0.8	−0.3	−0.6	0.0	−1.8	1.4	2.3	4.0	4.3
IIαB	10.5	11.8	12.7	11.1	12.8	11.2	14.3	14.1	16.5	16.9
IIαC	8.3	11.1	12.0	9.2	—	9.9	6.4	9.2	16.1	15.3
II$\alpha$$D_1$	5.0	10.6	9.2	13.8	14.3	10.2	14.9	17.3	17.5	15.6
II$\alpha$$D_2$	3.1	8.6	8.3	13.8	12.1	9.9	14.0	17.2	15.2	15.4
II$\alpha$$D_3$	2.6	7.3	—	11.3	7.3	6.3	8.0	15.2	—	15.2
IIIαX	16.1	19.4	22.4	18.8	20.8	17.9	18.1	19.7	21.9	22.4
IIIβX	2.6	5.9	8.9	5.3	7.3	4.4	4.6	6.2	8.4	8.9
IIIγX	−0.3	3.0	6.0	2.4	4.4	1.5	1.7	3.3	5.5	6.0
IIIδX	−0.5	2.8	5.8	2.2	4.2	1.3	1.5	3.1	5.3	5.8
IIIαA	14.7	15.1	15.6	15.3	15.9	14.1	17.3	18.2	19.9	20.2
IIIβA	1.2	1.6	2.1	1.8	2.4	0.6	3.8	4.7	6.4	6.7
IIIαB	12.9	14.2	15.1	13.5	15.2	13.6	16.7	16.5	18.9	19.3
IIIαC	10.7	13.5	14.4	11.6	—	12.3	8.8	11.6	18.5	17.7
III$\alpha$$D_1$	7.4	13.0	11.6	16.2	16.7	12.6	17.3	19.7	19.7	18.0
III$\alpha$$D_2$	5.5	11.0	10.7	16.2	14.5	12.3	16.4	19.6	17.6	17.8
III$\alpha$$D_3$	5.0	9.7	—	13.7	9.7	8.7	10.4	17.6	—	17.6

Experimental results for the Ar^{2+}-He (figures 1(*a*)-(*e*)) and Ar^{2+}-Ne (figure 1(*f*)) systems indicate the dominance of the reaction channels IαX, IIαX, IIIαX and IαX, IIαX respectively, at ΔE values between 3.0 and 7.8 eV. The broad endothermic structure at $\Delta E \leqslant -6$ eV is attributed to capture into excited states of Ar^+. The relative intensities of the excited states of Ar^{2+} in the incident beam can be reduced by decreasing the ionising electron energy E_e. For the Ar^{2+}-He system, this results in a gradual degradation of the peaks due primarily to IIIαX, but also to IIαX (shown in figures 1(*c*), (*d*) and (*e*) for E_e=52, 47 and 43 eV respectively). For $70 \leqslant E_e \leqslant 100$ eV, there were no perceivable changes in the spectra obtained, and hence no evidence of any

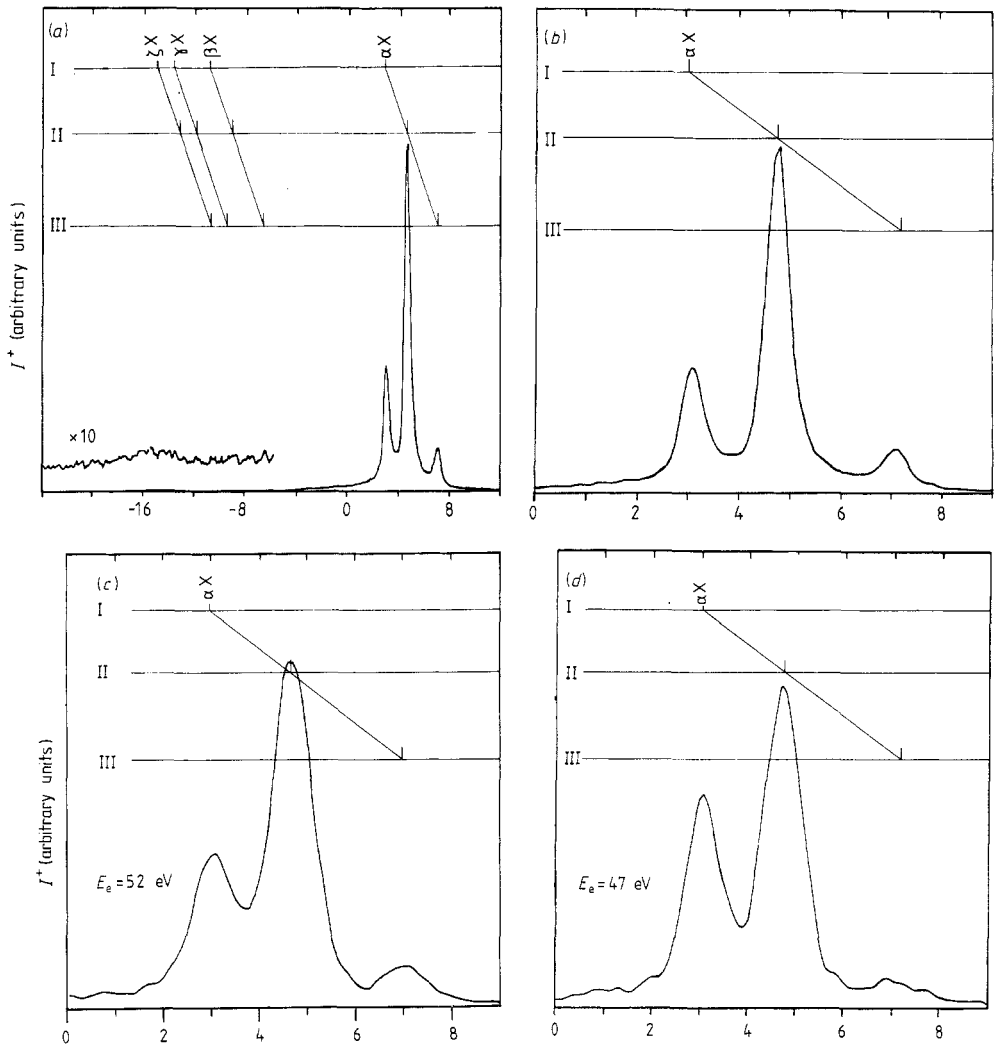

Figure 1. Translational-energy spectra of Ar^+ ions from 6 keV Ar^{2+}-He (*a*)-(*e*) and Ar^{2+}-Ne (*f*) collisions. The value of the ionising electron energy E_e is 100 eV unless otherwise stated.

long-lived highly excited electronic states of Ar^{2+} in the primary beam, contrary to the conclusions from the early works of Ast *et al* (1975) and Huber (1980). However, our results are in very good agreement with those of Lennon *et al* (1983) and Huber and Kahlert (1983).

Jellen-Wutte *et al* (1985) have investigated Ar^{2+}-He and Ar^{2+}-Ne single-electron capture collisions in the 0.5-5 keV impact energy domain. Their results at 5 keV compare favourably with our spectra; by varying the ionising electron energy E_e from 46 to 200 eV they have obtained analogous spectra to those shown in figure 1.

Using the transmission coefficient defined by Kimura *et al* (1984), 'reaction windows' for the Ar^{2+}-rare-gas systems can be estimated from the semiclassical curve crossing analysis of single-charge transfer processes formulated by Landau (1932),

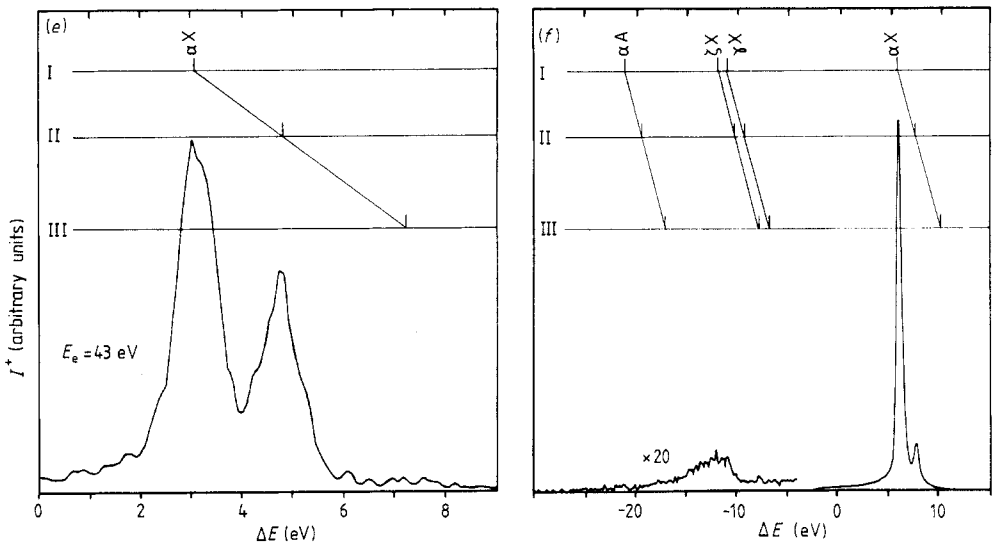

Figure 1. (continued)

Zener (1932) and Stückelberg (1932). The transmission coefficient $T(\gamma)$ takes the form

$$T(\gamma)=4(E_3(\gamma)-E_3(2\gamma))$$

where

$$E_n(x)=\int_1^\infty t^{-n}\,\mathrm{e}^{-xt}\,\mathrm{d}t \qquad n=0,1,2,\ldots$$

$$\gamma=2.05\times10^9 R_c^2 v^{-1}|f_{nl}|^2\exp(-0.96R_c I^{1/2})$$

where R_c is the curve crossing distance (in Å), v is the impact velocity (in ms^{-1}) and I is the ionisation energy of the target species (in eV). The fractional term $|f_{nl}|^2$ incorporated by Taulberg (1986) is given by

$$|f_{nl}|^2=(2l+1)[(n-1)!]^2[(n+l)!(n-l-1)!]^{-1}.$$

Here, n and l are the principal quantum numbers of the resultant electronic state of Ar^+. For capture into the ground state $3p^5\,{}^2P$ and the first excited state $3p^6\,{}^2S$ of Ar^+, $|f_{nl}|^2=0.5$. The reaction windows can now be parametrised in terms of the values $(M, L\text{-}H)$ of the energy defect ΔE (eV) at which $T(\gamma)$ maximises (M), and the range $(L\text{-}H)$ over which $T(\gamma)>0.2M$. For sufficiently large R_c

$$\Delta E=14.4R_c^{-1}.$$

The calculated reaction window parameters for 6 keV Ar^{2+}-He and Ar^{2+}-Ne collisions are (6.1, 4.8-7.4) and (5.6, 3.3-6.8) respectively, providing at least a qualitative interpretation of the present experimental data.

For Ar^{2+}-He, reference to table 4 indicates that the reaction channels IIαX and IIIαX lie at the boundaries of the reaction window as defined above. However, the energy defect for IαX is too low, and therefore the cross section for this channel is relatively small (figure 1(*b*)) despite the fact that ^3P is the most densely populated

state of the incident Ar^{2+} ion beam. Assuming that the metastable fractions f in the Ar^{2+} projectile beam are statistically determined, then $f(^3P):f(^1D):f(^1S)=9:5:1$.

For Ar^{2+}-Ne, the reaction window is shifted towards a lower energy defect. From table 4, we see that only $I\alpha X$ falls within the window defined by (5.6, 3.3-6.8). Consequently $I\alpha X$ dominates the capture spectrum (figure 1(f)). Channel $II\alpha X$ is also present, but at a much lower relative intensity (1:9) than that suggested by considering the relative statistical population of ^1D with respect to ^3P (5:9) in the primary Ar^{2+} ion beam.

For the Ar^{2+}-Ar, Ar^{2+}-Kr and Ar^{2+}-Xe systems (figure 2), table 4 indicates that there are no reaction channels available involving low-lying states of Ar^{2+} in their

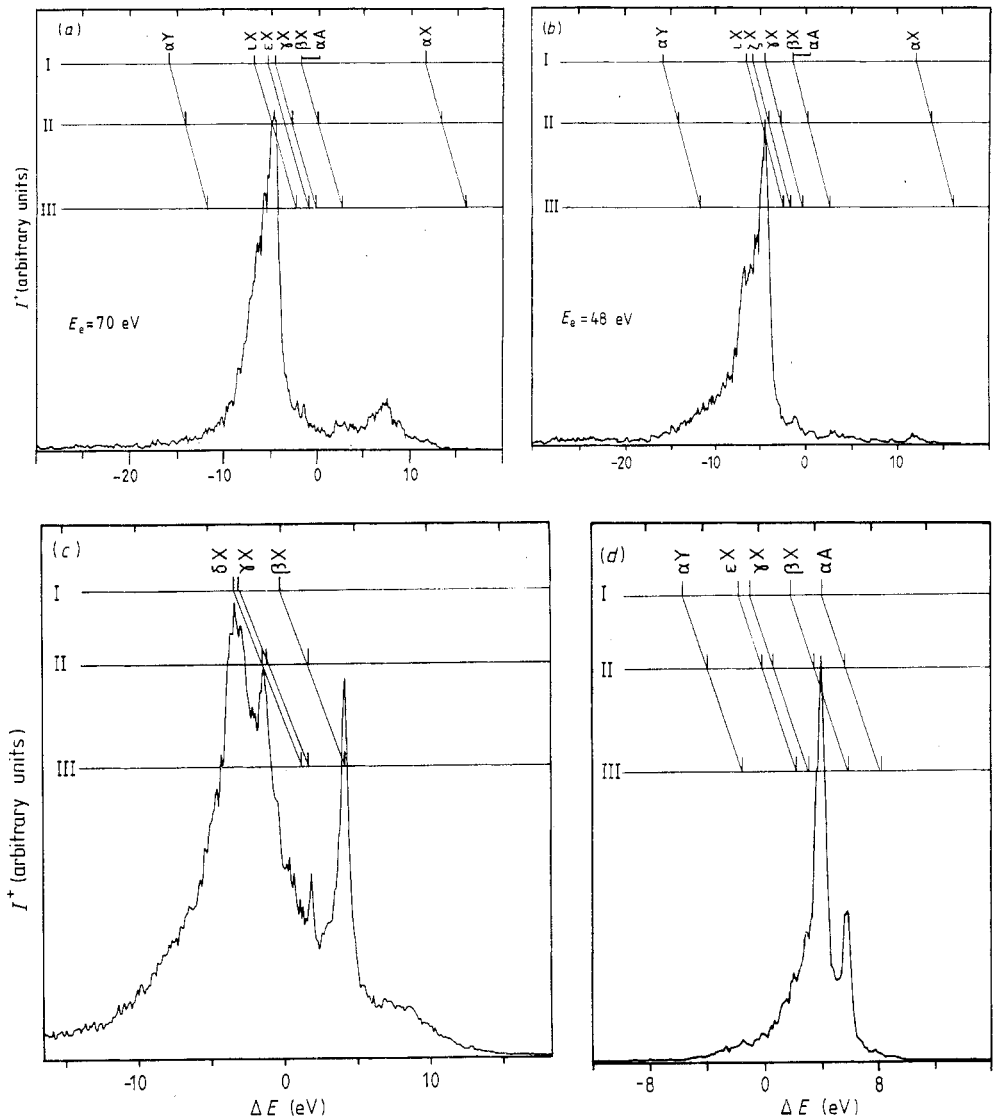

Figure 2. Translational-energy spectra of Ar^+ ions from 6 keV Ar^{2+}-Ar (a) and (b), Ar^{2+}-Kr (c) and Ar^{2+}-Xe (d). The value of the ionising electron energy E_e is 100 eV unless otherwise stated.

respective 'reaction windows' (4.7, 3.7-5.6), (4.3, 3.4-5.2) and (4.0, 3.1-4.7). Consequently, the maximum cross section is provided by non-crossing endothermic channels involving capture into excited electronic states of Ar^+. For Ar^{2+}-Ar, reduction of E_e (figure 2(*b*)) indicates the presence of IαX at a low signal level together with contributions from long-lived highly excited states of Ar^+ such as 3d $^5D^o$, 3d' $^3F^o$ and 3d'' $^3F^o$ with excitation energies from 18 to 23 eV. For Ar^{2+}-Kr, IIIβX falls at the maximum of the reaction window, explaining its narrow and prominent profile. As in all the systems studied, peak assignment is facilitated by accurate energy scale calibration and reduction of E_e to pinpoint processes involving the ground state Ar^{2+}. For Ar^{2+}-Xe, target excitation via IαA primarily provides a channel at a favourable crossing distance, and consequently a strong sharp peak.

One of the primary reasons for this reinvestigation of rare-gas targets was to establish reliable reference calibration systems for subsequent analysis of molecular targets. We now believe that previous discrepancies quoted in the literature are resolved. In particular, Ar^{2+}-Ne at $E_e \simeq 45$ eV exhibits one sharp peak ($\Delta E = 6.1$ eV) separate from the main processes observed for most molecular targets, thus making it a good calibration system.

Our results for Ar^{2+}-Ar, Ar^{2+}-Kr and Ar^{2+}-Xe disagree with those of Kamber *et al* (1982b) who attributed the dominant peaks in each case to ground-state-ground-state or near-ground-state transitions. For Ar^{2+}-Ar, good agreement is obtained with the work of Stevens *et al* (1983) at 2.9 keV impact energy once an energy scale calibration correction has been applied (see Lennon *et al* 1983). The results of Puerta and Huber (1985) for Ar^{2+}-Ar also agree with the present assignments, resolving earlier discrepancies.

2.2. *Ar^{2+}-molecular-target collision systems*

Table 5 shows the energy defects for the most probable reaction channels for collisions of Ar^{2+} with molecular targets. The number of possible exit channels for electron capture are greatly increased when molecular targets are substituted for atoms because vibrational excitation and dissociation have to considered.

Translational-energy scale calibration was performed by using rare-gas targets as a standard. Furthermore, accurate calibration was facilitated by mixing the molecular target under study with Ne in appropriate quantities so as to enable both the Ar^{2+}-molecular-target and Ar^{2+}-Ne spectra to be recorded simultaneously. Errors in ΔE after calibration by this technique are always less than ± 0.2 eV.

For Ar^{2+}-O_2 and Ar^{2+}-NO, the energy levels of the O_2^+ and NO^+, respectively, are such that the peaks due to reactions IβX, IIβX and IIIβX appear in the spectra free from other reactions which also fall within the reaction window. These spectra are shown in figure 3; the main processes appear as sharp peaks of the same form as in the Ar^{2+}-He and Ar^{2+}-Ne spectra. For Ar^{2+}-O_2 the high-energy peak at $\Delta E = 8$ eV is attributed to target dissociation, whereas the peak at $\Delta E \simeq 2$ eV for Ar^{2+}-NO could be due to capture to excited states of Ar^+. On the other hand, for Ar^{2+}-N_2 (see figure 3(*c*)), βX processes are more endothermic. The spectrum is dominated by a single broad peak due to target dissociation via IαD or target excitation to the D $^2\Pi_g$ state of N_2^+ (approximately 7 eV above the ground state, which is not tabulated in table 3), with a possible contribution from IIIβX at comparable values of ΔE. The broader low-intensity structure at $\Delta E \simeq -6$ eV is attributed to capture into higher excited states

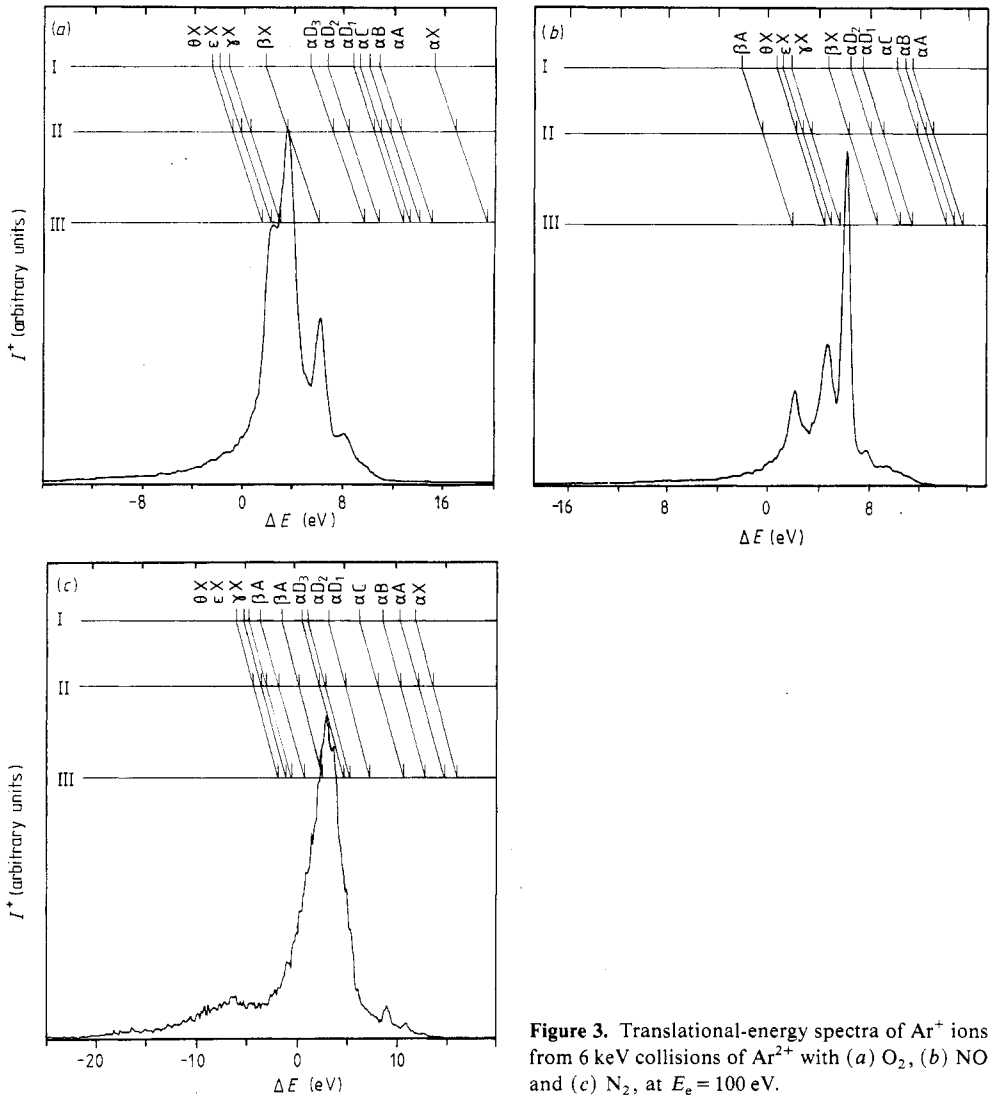

Figure 3. Translational-energy spectra of Ar^+ ions from 6 keV collisions of Ar^{2+} with (*a*) O_2, (*b*) NO and (*c*) N_2, at $E_e = 100$ eV.

of Ar^+. Weak peaks on the high-energy side are due to successive target excitation through channels IαX, IαA and IαB. This assignment agrees with that of Neuschäfer *et al* (1979) who investigated the single-electron capture Ar^{2+}-N_2 system at low impact energies (2-25 eV), finding that the translational energy distribution of Ar^+ is dominated by a broad peak at $\Delta E \simeq 4.5$ eV due to the formation of $N_2^+(D\ ^2\Pi_g)$.

Target excitation is evident once again for Ar^{2+}-NH_3 and Ar^{2+}-CO_2, the spectra for which are very similar (figure 4). The main process involves formation of N^+ and C^+ respectively. Strong tailing on the low-energy side is due to capture to excited states of Ar^+. The two narrow peaks at $\Delta E \simeq 8$ eV, for Ar^{2+}-CO_2, are due to IαB and IαA, whereas the broad peak centred near $\Delta E = 12$ eV indicates further target dissociation. The capture cross section for Ar^{2+}-N_2O is very low, again because there is not an easily accessible reaction channel in the $3 \leqslant \Delta E \leqslant 8$ eV range. The variation of the

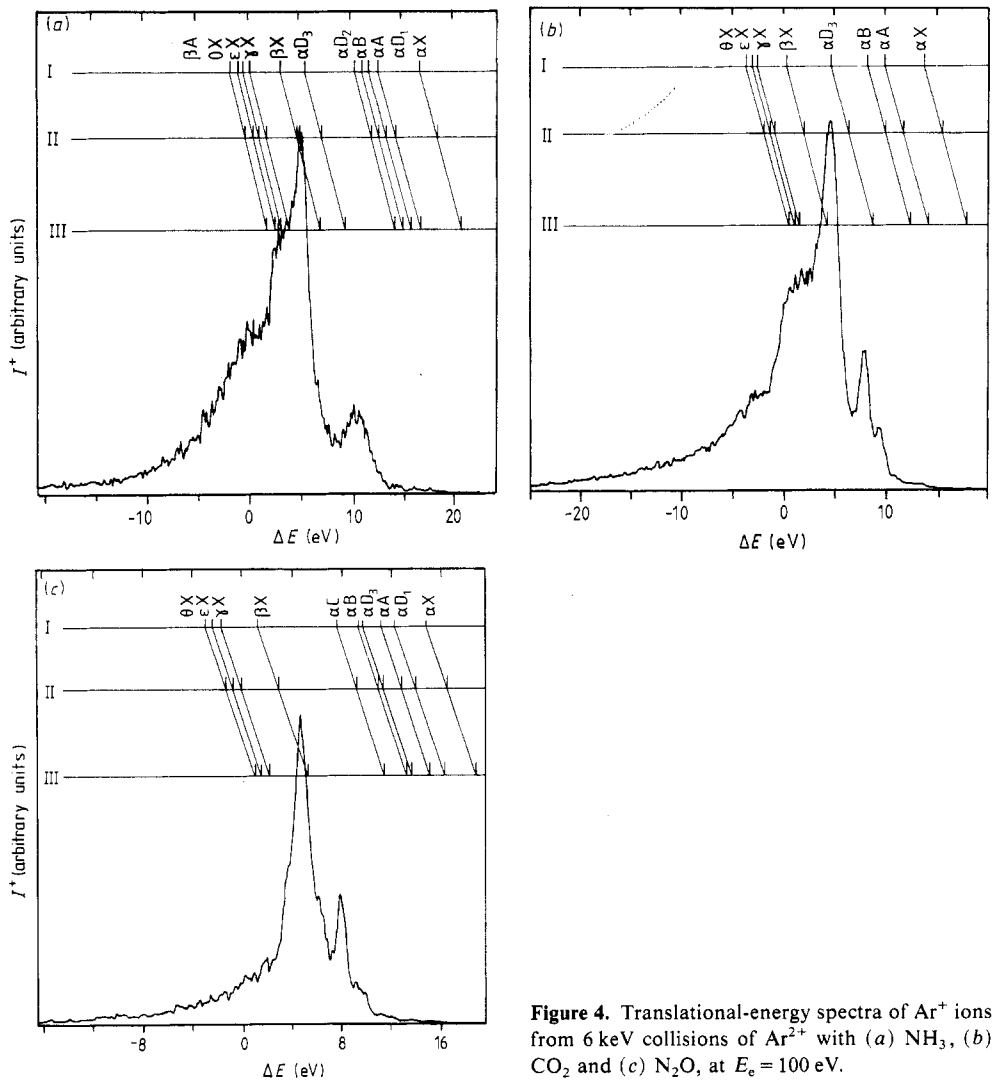

Figure 4. Translational-energy spectra of Ar^+ ions from 6 keV collisions of Ar^{2+} with (*a*) NH_3, (*b*) CO_2 and (*c*) N_2O, at $E_e = 100$ eV.

ionising electron energy shows that IIIβX, at $\Delta E = 5.3$ eV, is not present. High-energy peaks in figure 4(*c*) can be attributed to IαC, IαB and to target dissociation, which probably accounts for the base peak at $\Delta E = 4.5$ eV, although this is by no means clear from the present data.

Ar^{2+}-hydrocarbon single-electron capture systems exhibit a number of interesting features (figure 5) and will be reported in a future publication. The Ar^{2+}-CH_4 and Ar^{2+}-C_2H_6 spectra show the same general trends of target excitation and dissociation as reported above for small targets. Ar^{2+}-1-C_4H_8 (figure 5(*c*)) and Ar^{2+}-C_6H_6 (figure 5(*d*)) demonstrate a quite different behaviour, attributed to the multi-electron target structure, providing a high density of states. The availability of so many favourable channels with $3.0 \leqslant \Delta E \leqslant 7.0$ eV produces one intense broad peak, reflecting the electron capture window for that particular system. We believe the second, sharper peak at

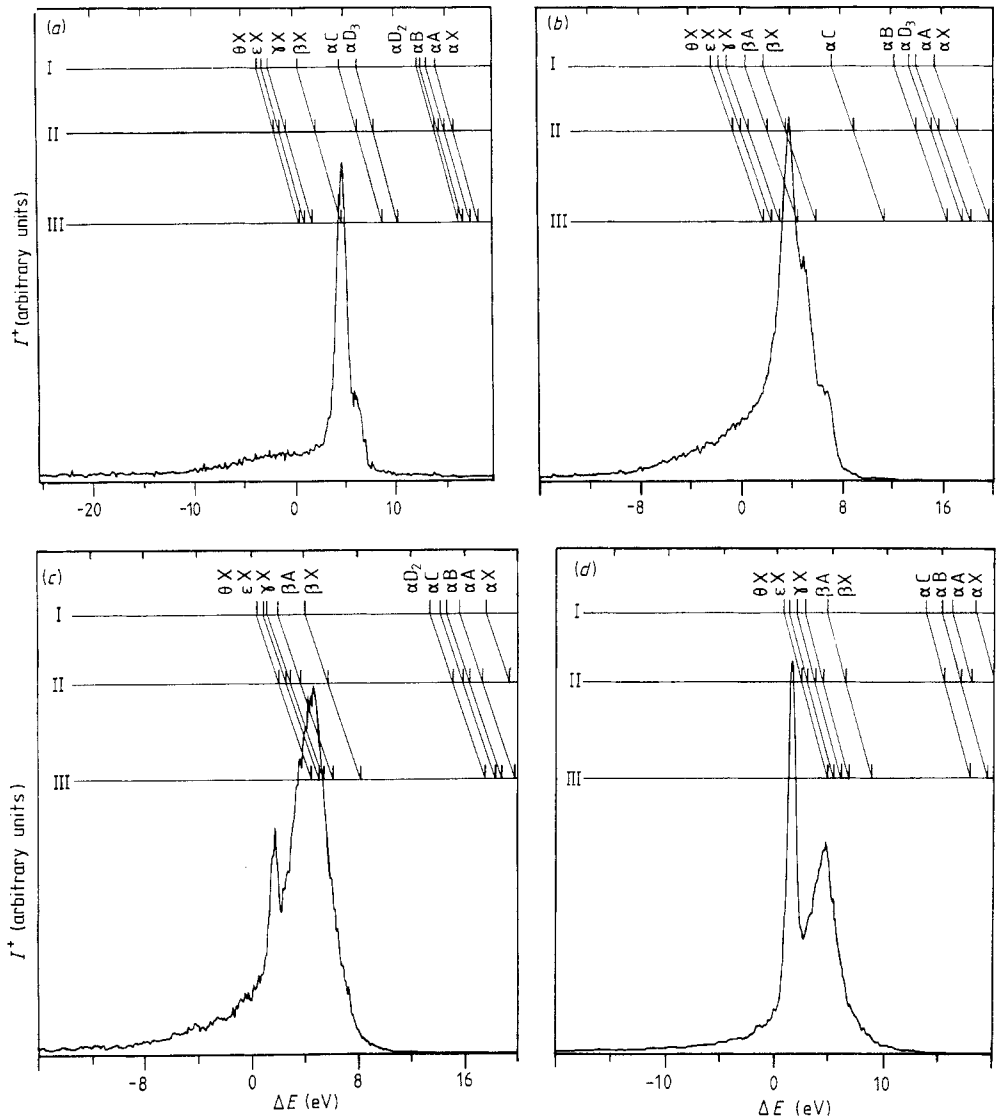

Figure 5. Translational-energy spectra of Ar^+ ions from 6 keV collisions of Ar^{2+} with (*a*) CH_4, (*b*) C_2H_6, (*c*) 1-C_4H_8 and (*d*) C_6H_6 (benzene), at $E_e = 100$ eV.

$\Delta E \simeq 2$ eV, is due to electron capture from carbon–carbon multiple bonds involving delocalised electrons—for example, in π orbitals.

3. Conclusion

Previously reported results for Ar^{2+}–rare-gas systems have been re-examined and the corresponding reaction channel assignments clarified. This was necessary in order to have reliable calibration spectra for use with molecular targets where the lack of easily identifiable features makes direct reaction assignment virtually impossible. Our data

clearly indicate collisions involving capture into excited states of Ar^+ for each of the Ar, Kr and Xe targets, together with the presence of excited states in the Ar^{2+} projectile beam. These latter spectral features were confirmed by the variation in the ionising electron energy, notably for Ar^{2+}-He. After this detailed study, we believe that the energy scale calibration is now accurate to less than 0.5 eV.

Target excitation was significant for Ar^{2+}-Xe and for most of the molecular targets considered which also underwent considerable dissociation, for example, Ar^{2+}-NH_3 and Ar^{2+}-CO_2. The general feature of Ar^{2+}-hydrocarbon spectra was a broad peak, due to the high density of target electronic states, located at $\Delta E \simeq 5$ eV, whose intensity increased with increasing hydrocarbon mass, mirroring the capture window for such systems.

For all the targets studied, the maximum cross section occurred for reaction channels with an energy defect ΔE in the range $3.0 \leqslant \Delta E \leqslant 7.0$ eV. This signifies the crossing of potential-energy surfaces of the entrance and exit channels at internuclear distances between 2 and 5 Å.

Evidence of capture of delocalised electrons from unsaturated hydrocarbons was detected for Ar^{2+}-1-C_4H_8 and Ar^{2+}-C_6H_6, and is the subject of further investigation.

Acknowledgments

We wish to thank University College Swansea for financial support. PJ is indebted to the SERC for the award of a postgraduate studentship and EYK thanks the Royal Society for a postdoctoral assistantship.

References

Ast T, Terwilliger D T, Beynon J H and Cooks R G 1975 *J. Chem. Phys.* **62** 3855-63
Butler S E, Heil T G and Dalgarno A 1980 *Astrophys. J.* **241** 442-7
Eland J H D 1984 *Photoelectron Spectroscopy* (London: Butterworths)
Huber B A 1980 *J. Phys. B: At. Mol. Phys.* **13** 809-18
Huber B A and Kahlert H-J 1983 *J. Phys. B: At. Mol. Phys.* **16** 4655-69
Jellen-Wutte U, Schweinzer J, Vanek W and Winter H 1985 *J. Phys. B: At. Mol. Phys.* **18** L779
Kamber E Y, Mathur D and Hasted J B 1982a *J. Phys. B: At. Mol. Phys.* **15** 263-73
—— 1982b *J. Phys. B: At. Mol. Phys.* **15** 2051-9
Kimura M, Iwai T, Kaneko Y, Kabayashi N, Matsumoto A, Ohtani S, Okuno K, Takagi S, Tawara H and Tsurubuchi S 1984 *J. Phys. Soc. Japan* **53** 2224
Kimura K, Katsumata S, Achiba Y, Yamazaki T and Iwata S 1981 *Handbook of He I Photoelectron Spectra of Fundamental Organic Molecules* (Tokyo: Japan Scientific Societies)
Landau L D 1932 *Z. Phys.* **1** 88
Lennon M, McCullough R W and Gilbody H B 1983 *J. Phys. B: At. Mol. Phys.* **16** 2191-204
Levin R D and Lias S G 1982 *Ionisation Potential and Appearance Potential Measurements 1971-1981* NSRDS-NBS71 (Washington, DC: US Govt Printing Office)
Moore C E 1971 *Atomic Energy Levels* NBS Circular No 467 (Washington, DC: US Govt Printing Office)
Morgan R P, Beynon J H, Bateman R and Green B N 1978 *Int. J. Mass Spectrom. Ion Phys.* **28** 171-91
Neuschäfer D, Ottinger C H, Zimmerman S, Lindinger W, Howorka F and Störi H 1979 *Int. J. Mass Spectrom. Ion Phys.* **31** 345-65
Puerta J and Huber B A 1985 *J. Phys. B: At. Mol. Phys.* **18** 4445-53
Rabalais J W 1977 *Principles of Ultraviolet Spectroscopy* (New York: Wiley)
Robinson J W 1974 *CRC Handbook of Spectroscopy* (Boca Raton, Fl: CRC)
Smith D, Grief D and Adams N G 1979 *Int. J. Mass Spectrom. Ion Phys.* **28** 171-91

Stevens J, Peterson R S and Pollack E 1983 *Phys. Rev.* A **27** 2396-402
Stückelberg E C G 1932 *Helv. Phys. Acta* **5** 320
Taulberg K 1986 *J. Phys. B: At. Mol. Phys.* **19** L367
Turner D W, Baker A D, Baker C and Brundle C R 1970 *Molecular Photoelectron Spectroscopy* (London: Wiley)
Zener C 1932 *Proc. R. Soc.* A **137** 696